Available online at www.sciencedirect.com

jmr&t Journal of Materials Research and Technology

journal homepage: www.elsevier.com/locate/jmrt

Original Article

Hydrogen embrittlement behavior in FeCCrNiBSi TRIP steel

Ehsan Norouzi [a], Reza Miresmaeili [a,*], Hamid Reza Shahverdi [a], Mohsen Askari-Paykani [a], Laura Maria Vergani [b]

[a] Department of Materials Engineering, Tarbiat Modares University, Jalal Ale Ahmad Highway, P.O. BOX 14115-143, Tehran, Tehran, Iran

[b] Department of Mechanical Engineering (DMEC), Politecnico di Milano, Via La Masa 1, 20156 Milano, Italy

ARTICLE INFO

Article history:
Received 1 December 2022
Accepted 9 January 2023
Available online 13 January 2023

Keywords:
Hydrogen embrittlement
Plastic deformation
Martensite transformation
Dislocation

ABSTRACT

The effect of plastic deformations on the hydrogen embrittlement (HE) of transformation-induced plasticity (TRIP) steel was studied. In situ tensile tests showed that with increasing hydrogen current density, total elongation loss was raised to 36.8% as compared to an uncharged specimen. The electron backscatter diffraction (EBSD) observation indicated that hydrogen charging decreased stacking fault energy (SFE), resulting in the formation of more α′- martensite by both indirect and direct transformation. The α′- martensite volume fraction at the same degree of deformation in uncharged and charged samples was 31% and 39%, respectively. With plastic deformation, reversible trap sites were raised because of the increased dislocation density and the formation of α′- martensite, which was obtained from EBSD characterization and had a good correlation with the results of the thermal desorption spectroscopy (TDS) analysis.

1. Introduction

Transformation-induced plasticity (TRIP)-assisted steels are advanced high strength steels, which are widely used to make components in the automotive and construction industries because they have high strength-elongation properties, are easy to form, and are inexpensive to produce [1,2]. TRIP steels enable a significant reduction in raw structural mass, which helps reduce the weight of vehicle and improves its passive safety [3–5].There is the problem of the hydrogen induced cracking and embrittlement in the automotive industry, for which TRIP steels are very desirable owing to their high strength. Hydrogen absorption may occur in the steel-making or automobile-manufacturing processes due to the great mobility of the hydrogen atom in the steel microstructure [6,7]. During an automobile's service life, both environment-assisted corrosion and hydrogen-induced cracking (HIC) are possible occurrences. TRIP steels can trap varying amounts of hydrogen with varying degrees of permeability and solubility, making it challenging to evaluate their HE behavior [8,9]. Microstructure control and optimization are essential to understand the relationship between microstructure and mechanical performance of TRIP steels in the presence of

* Corresponding author.
E-mail address: miresmaeili@modares.ac.ir (R. Miresmaeili).

https://doi.org/10.1016/j.jmrt.2023.01.052

hydrogen. For steels with a low stacking fault energy (SFE), two potential transformation sequences might occur during deformation-induced martensitic transformation: austenite (γ) → bcc-martensite (α') and γ → hcp-martensite (ε) → α'. Metastable austenitic CrNi steels with SFE >20 mJ/m^2 undergo directly into α'-martensite, while those with SFE <20 mJ/m^2 transform indirectly into α'-martensite [10,11].

Researchers have recently investigated the hydrogen embrittlement of TRIP steels and metastable austenitic steels. According to Ryu et al. [12], hydrogen deteriorates mechanical properties after the martensite transformation because martensite has a greater hydrogen diffusivity than austenite. Fussik et al. [13] found a considerable increase in the content of α'-martensite after hydrogen charging. They concluded that hydrogen can reduce SFE, which promotes the direct and indirect transformation of austenite to α'-martensite. Two variables govern α'- martensite's effect on HE: First, α'-martensite is a brittle and hard phase; second, the hydrogen diffusivity in α'-martensite (BCC) is roughly five times as high as that in austenite (FCC) [14]. Luppo and Ovejero-Garcia [15] reported that the martensite phase has the lowest hydrogen embrittlement resistance and introduced it as a reversible trapping site. TRIP steels exhibited more ductility loss owing to hydrogen embrittlement than steels that did not transform upon plastic deformation [16]. Hilditch et al. [17] stated that there were no significant changes in the yield strength and strain hardening behavior of TRIP780 in the presence of hydrogen. Lovicu et al. [18] confirmed that the great sensitivity of TRIP steel to hydrogen is due to the severe embrittlement of the stress produced by martensite. Rozenak et al. [19] discovered that hydrogen influenced the stability of austenite and resulted in the induced transition of austenite to martensite. Crack initiation in TRIP steels has always been correlated to the presence of martensite, as revealed by Lacroix et al. [20]. TRIP steels suffer significant mechanical deterioration when exposed to much lower levels of hydrogen [21].

Limited research has been conducted on the link between α'-martensite, ε-martensite and hydrogen during deformation. The effect of hydrogen on TRIP is still poorly known, and the role of hydrogen in the deformation mechanisms of TRIP steel needs further investigation. The current research focuses on the influence of hydrogen on the mechanical properties and the transformation of austenite to martensite (TRIP effect). For this purpose, the mechanical properties at different current densities during hydrogen charging were investigated. In addition, the effects of hydrogen on the microstructure of the deformed TRIP steel were evaluated at certain strain levels.

2. Experimental procedure

After grinding the sample surfaces with 60–2000 Sic papers, the specimens were electrochemically pre-charged in an aqueous NaOH solution at current densities of 10 and 30 mA/cm^2 for 20 h. The tensile of in-situ electrochemical hydrogen charging was tested immediately after pre-charging at the same condition. For this purpose, a special cell and a tensile fixture were mounted. A small specimen with the a gauge length nominal dimension of 11.4 × 3 × 1 mm was used in this investigation [22]. All specimens were tested with an Instron device at a maximum load of 20 tons and a tensile speed of 0.1 mm/min. Each condition was evaluated using a minimum of three samples. The interrupted tensile tests were stopped at 21% strain for the uncharged sample and 12% strain for the charged and uncharged conditions to characterize the deformation mechanism by electron backscatter diffraction (EBSD). The cross-sections of the specimens obtained from the interrupted tensile tests were prepared with carbide paper (600, 1200, and 2500 grit) and diamond polishing (3 and 1 μm). The specimens were prepared by electrochemical polishing with 94% acetic acid and 6% perchloric acid for EBSD measurements. Microstructures were studied using scanning electron microscopy (SEM) and EBSD with a step size of 0.08 μm, accelerating voltage of 20 KV, probe current of 10 nA, a tilt angle of 70° and working distance of 12 mm. The EBSD data was analyzed using the HKL-Channel 5 system. The quantity of diffusible hydrogen in the H-charged specimens was calculated using thermal desorption spectroscopy (TDS). The activation energy was calculated using heating rates of 5, 10, and 20 °C/min.

3. Results

3.1. Mechanical characteristics and initial microstructure

Fig. 1 presents stress-strain diagrams for uncharged and charged specimens. For the H-free specimen, the yield strength is 1186 MPa, and ultimate tensile strength (UTS) is 942 MPa, whereas the UTSs of the specimens charged at 10 and 30 mA/cm^2 are 1165 MPa and 1126 MPa and their yield strengths are 939 MPa and 936 MPa, respectively, indicating that hydrogen has slight influence on the yield strength. To quantify tensile ductility, the HE sensitivity parameter (I_{HE}) was derived using equation (1):

$$I_{HE}\ (\%) = (1 - E_H / E_0) \times 100\% \quad (1)$$

Where E_0 represents the material's elongation before hydrogen charging and E_H denotes the material's elongation after hydrogen charging. A greater I_{HE} value suggests that HE resistance is low. The mechanical properties are summarized in Table 1.

Fig. 2 shows the EBSD image of the microstructure before hydrogen charging by EBSD. This microstructure is composed of austenite, $Cr_{23}C_6$, and Cr_2B, and there is no evidence of the martensite phase.

3.2. Microstructure evaluation

The EBSD results of interrupted tensile tests are shown in Fig. 3a–f. The inverse pole figure and phase map of an interrupted tensile test specimen in the air just before the fracture (21% strain) are shown in Fig. 3a and b. It can be observed in Fig. 3b that direct transformation γ (FCC) → α' (BCC) occurred without any intermediate phase of ε-martensite. Fig. 3c and d presents the EBSD maps of the interrupted tensile specimen after hydrogen charged at 30 mA/cm^2 just before fracture (12% strain). The findings revealed that austenite, α'-martensite,

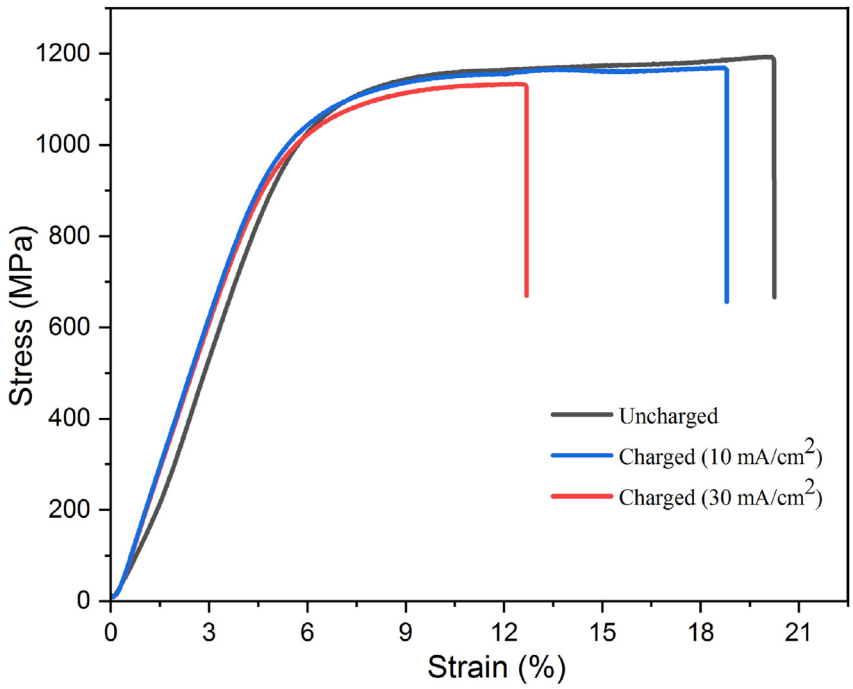

Fig. 1 – Tensile engineering stress–strain curves before and after hydrogen charging.

Table 1 – The mechanical characteristics with and without hydrogen charging.

Specimen designation	Yield Strengh (MPa)	Tensile Strengh (MPa)	Total Elongation (%)	Reduction of area (%)	Tensile strength loss due to H I_s (%)	Total elongation loss due to H I_{HE} (%)
Uncharged	942	1186	20.2	65.2	–	–
H-Charged at 10 mA/cm^2	939	1165	18.8	63.2	1.7	6.9
H-Charged at 30 mA/cm^2	936	1126	12.6	38.4	5	36.8

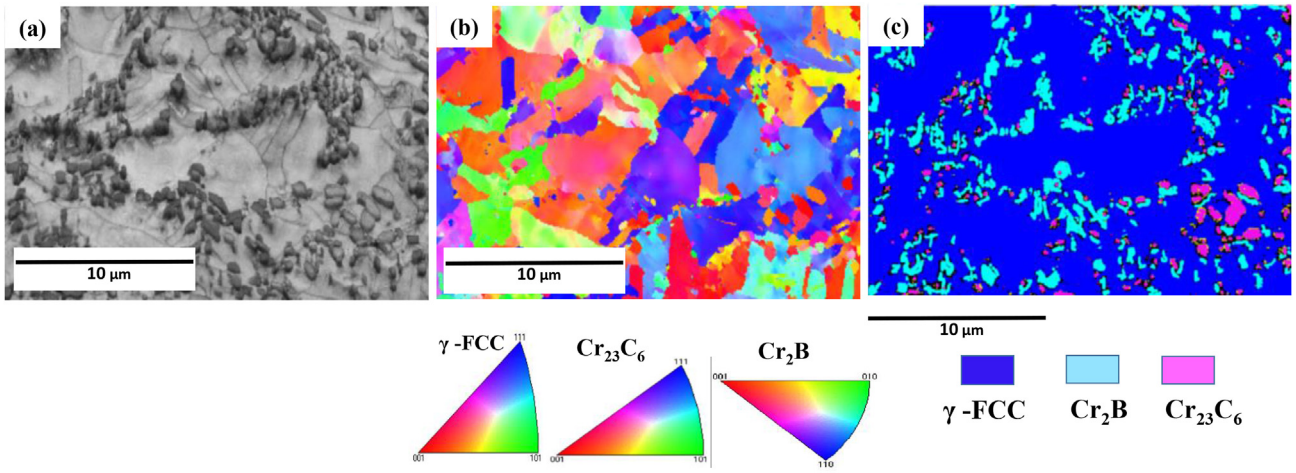

Fig. 2 – (a) The SEM image, (b) inverse pole figure (IPF), and (c) phase map of TRIP steel.

and ε-martensite percentages were 47%, 39%, and 4%, respectively. It can be seen that austenite can be directly and indirectly (γ → ε→ α′) transformed to α′-martensite in the presence of hydrogen. Interrupted tensile test specimen in the air at a strain of 12%, consisting of 58% austenite and 31% α′-martensite (Fig. 3e and f), is compared to the interrupted

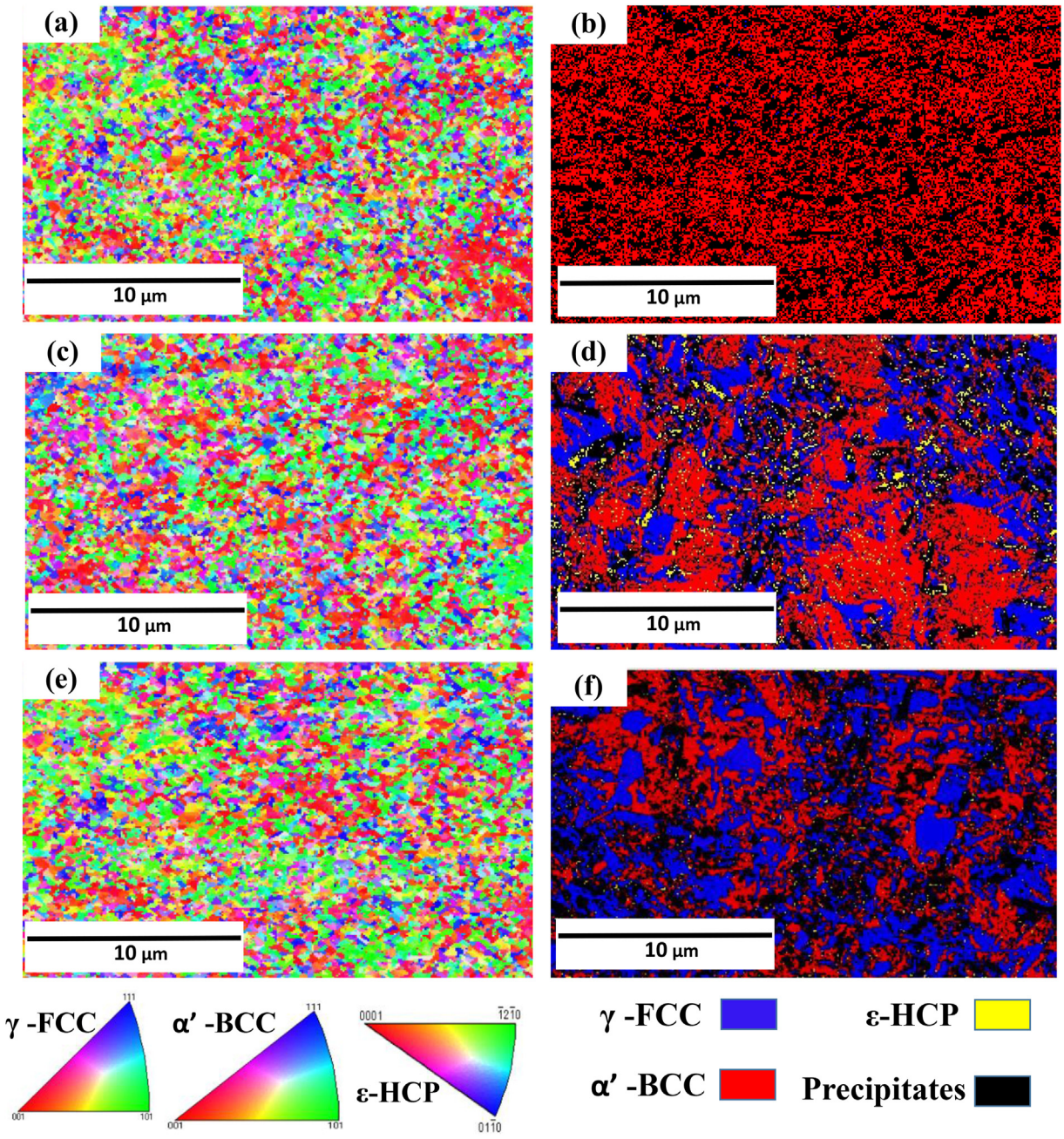

Fig. 3 – The EBSD images of pole figure and phase maps for strained microstructure with and without hydrogen charging, a,b: strained specimens in the air before fracture (21% strain), c,d: strained specimens in hydrogen before fracture (12% strain), e,f: strained specimen in the air up to 12% strain (at fracture strain of charged sample).

tensile specimen in hydrogen at the same strain in Fig. 3c and d. It can be deduced that the volume fractions of α′-martensite was greater in the H-charged specimens than in the H-free one at same deformation (12% strain).

Fig. 4a–f shows the maps of kernel average misorientation (KAM) for the deformed specimens. KAM is obtained directly from the EBSD data. KAM parameters provide information about the value of local deformation, which corresponds to the level of dislocation density. Due to the more plastic deformation, the KAM value of the uncharged specimen (21% strain) was larger than that of the other specimens (Fig. 4a and b). As shown in Fig. 4 c-f, it was obvious that the charged specimen exhibited a higher KAM value than the uncharged sample in both the austenite and martensite phases at the same strain of 12%.

Fig. 5 illustrates the crack initiation and propagation of the H-charged sample after the tensile test. Many transgranular or intergranular fractures traverse the γ-FCC/α′-BCC and γ-FCC/Cr_2B interfaces. Hydrogen tends to be diffused preferentially at interphase boundaries between two phases, providing a

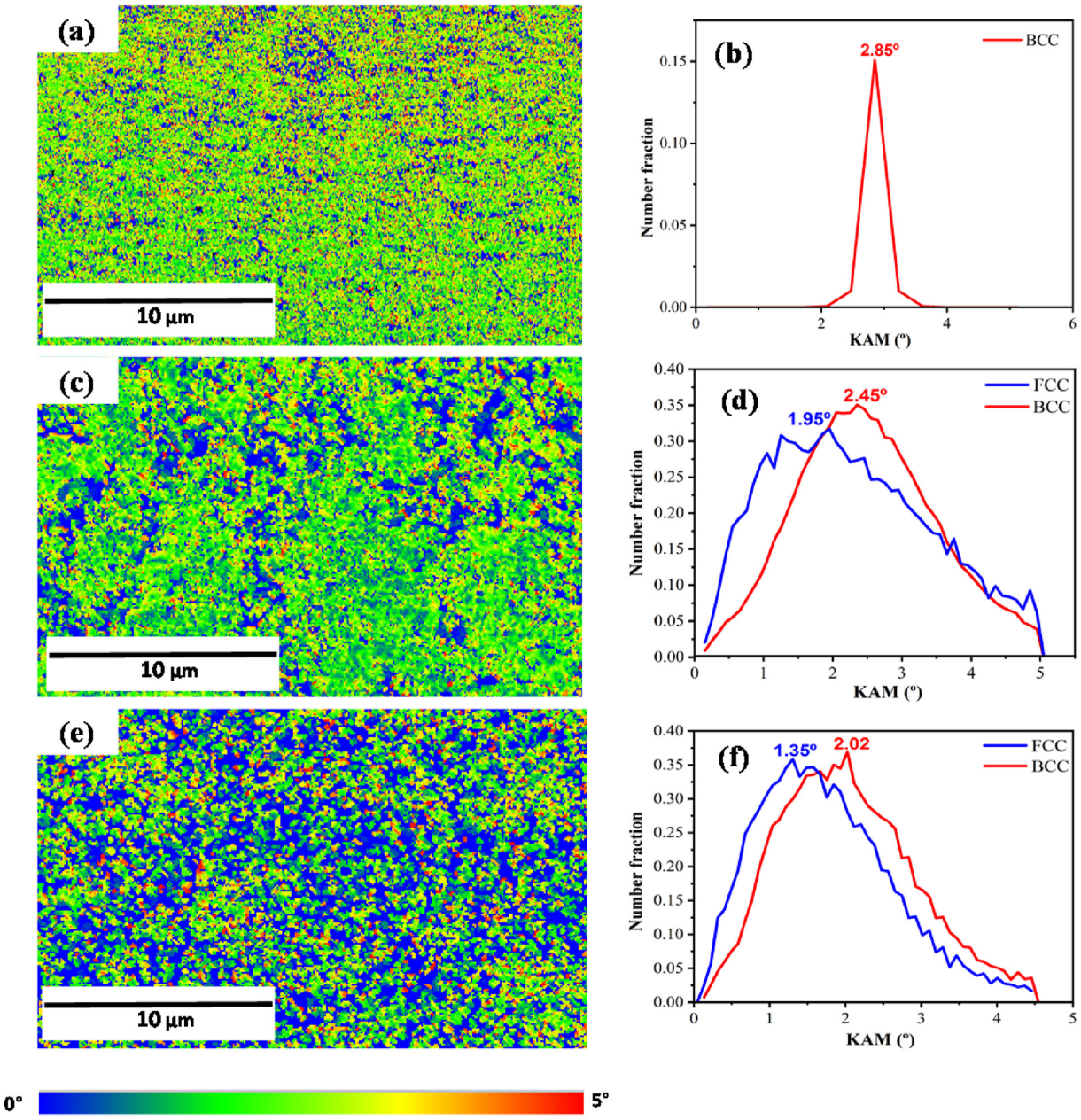

Fig. 4 – The KAM maps relative fraction and distribution (ranging 0–5° marked by rainbow color), (a),(b) strained specimen in the air before fracture, (c),(d) strained specimen in presence of hydrogen before fracture (12% strain), (e) (f) strained specimen in the air up to 12% strain (at fracture strain of charged sample).

local hydrogen concentration region. In other words, hydrogen diffusion caused interatomic bonds to weaken during deformation. The difference in hydrogen diffusivity and solubility between matrix (austenite) and phases could cause high stress concentration, which is of important for propagation of crack.

3.3. *Thermal desorption spectroscopy (TDS) analysis*

Fig. 6 shows the hydrogen content in undeformed and deformed specimens at various heating rates of 5, 10, and 20 °C/min. In the deformed (12% strain) and undeformed specimens, there are three peaks for all heating rates. One peak is below 300 °C and two peaks are above 300 °C (Fig. 6a and b.). Equation (2) [23] can be used to figure out the activation energies of TDS peaks and link them to microstructure properties:

$$\frac{d\left(\ln\frac{\varphi}{T_{max}^2}\right)}{d\left(\frac{1}{T_{max}}\right)} = -\frac{E_a}{R} \quad (2)$$

Where φ denotes the rate of heating (K/min), T_{max} represents the highest temperature (°K), E_a (J/mol) indicates the activation energy and R shows the gas constant. Ea is calculated from a plot of ln (Φ/T2max) versus ln (1/Tmax) as shown in Fig. 7.

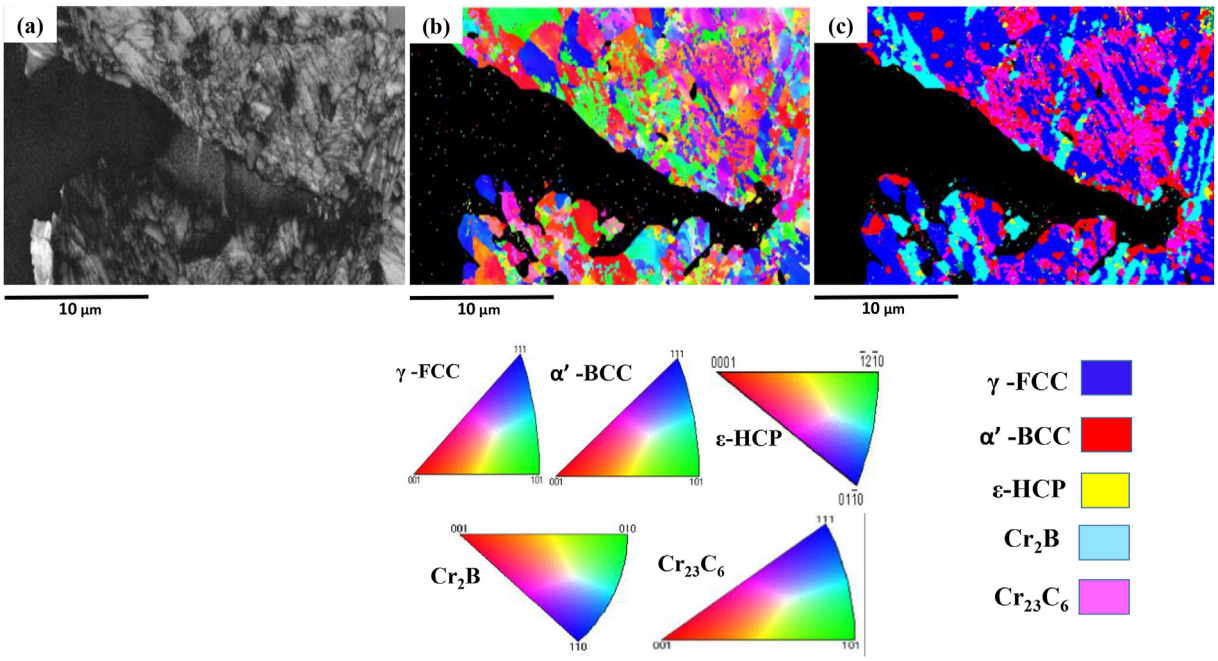

Fig. 5 – The morphology of the crack beneath the fracture surface after hydrogen charging. (a) SEM, (b) inverse pole figure (IPF), (c) phase map.

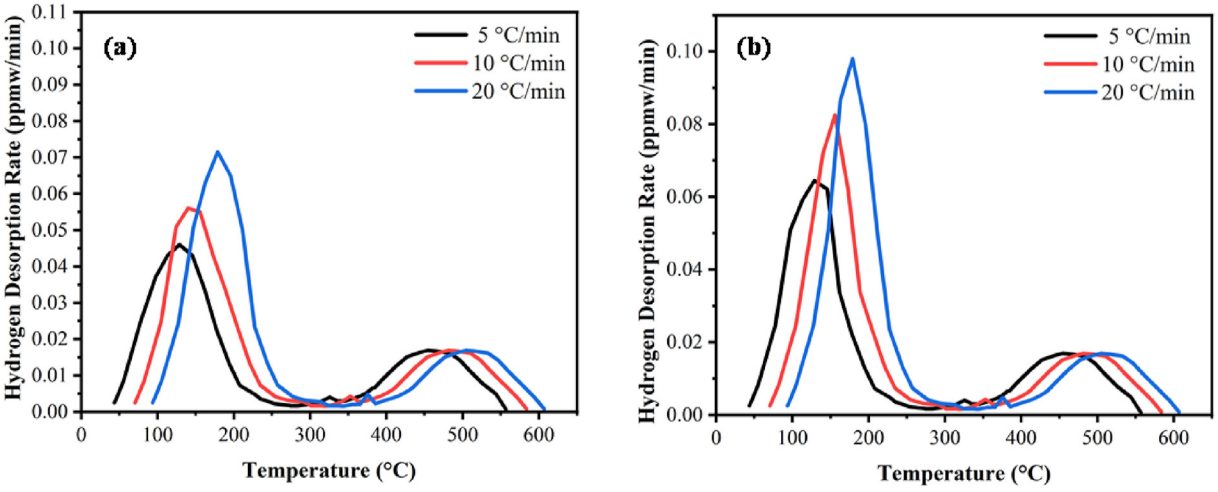

Fig. 6 – The TDS analysis of hydrogen desorption rate for various heating rates. (a) undeformed, (b) deformed (12% strain).

Fig. 7 illustrates the linear fitting of three peaks for the undeformed and deformed specimens, and Table 2 indicates the activation energy or their slopes obtained for the peaks.

4. Discussion

With respect to effect of hydrogen on the strength, the yield strength of samples decreased slightly after hydrogen charging. The occurrence of softening effect is due to the shielding effect of hydrogen, which decreased the critical shear stress for dislocation glide [24]. The presence of hydrogen was responsible for the loss of strength in the charged specimen. In addition, the effect of current density on elongation is shown in Table 1, which shows that the total elongation loss was increased by 6.9% for charged specimens at 10 mA/cm^2, and by 36.8% at 30 mA/cm^2. The higher the current density, the greater the elongation loss. The results are agree with those of Enos et al. [25] and Wang et al. [26]. One of the most well-acknowledged HE processes is hydrogen enhanced decohesion (HEDE), according to which the atomic bonding force and the surface energy diminish because of the

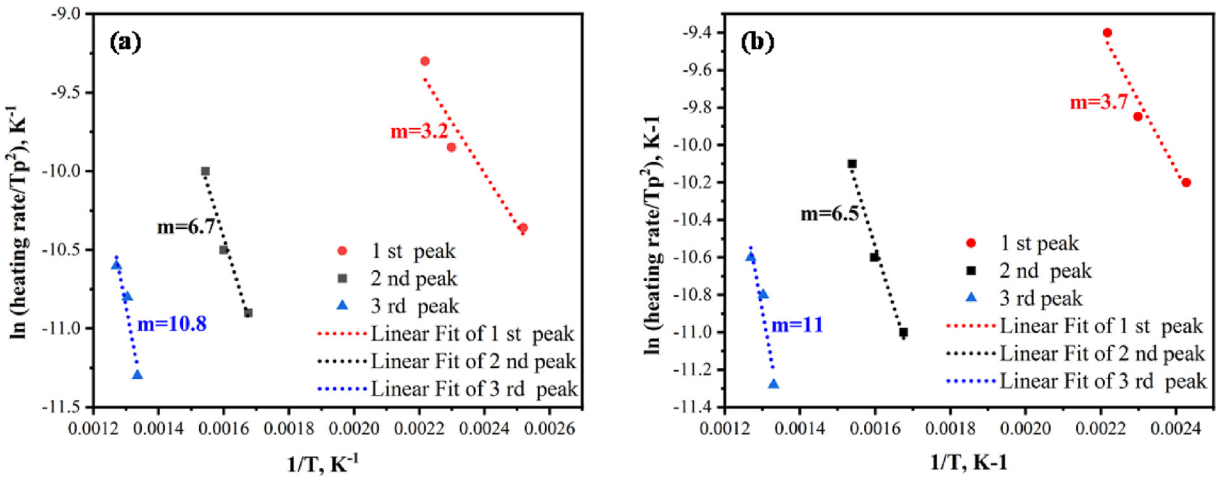

Fig. 7 – The peaks' linear fit as a function of heating rate. (a) undeformed, (b) deformed (12% strain).

Table 2 – The activation energy calculation parameters.

Heating rate (°C/min)	Peak temperature (°C)			Activation energy (kJ/mol)
	5	10	20	
Undeformed				
1st peak	124	147	178	26.6
2nd peak	334	355	375	55.6
3rd peak	476	494	514	89.7
Deformed (12%)				
1st peak	139	162	178	30.7
2nd peak	334	356	377	53.9
3rd peak	479	495	515	91.4

presence of solute hydrogen. The considerable loss of ductility in H-charged specimens compared to the H-free specimen in Table 1 and Fig. 1 could be ascribed to the presence of more α′-martensite in the charged specimen. Austenite is a powerful site of trapping hydrogen owing to its greater hydrogen solubility and lower hydrogen diffusivity compared to the other phases of steel. According to Hirth [27], when charged austenite undergoes transformation, the hydrogen is absorbed by freshly produced martensite, which is the most vulnerable to HE. When phase transformation occurs, a hydrogen-supersaturated martensite is formed, significantly increasing the hydrogen diffusivity. The great sensitivity of TRIP steel to hydrogen is correlated with martensite's severe embrittlement once subjected to stress [18]. It has also been reported that α′-martensite is a brittle and hard phase that enhances hydrogen diffusivity and acts as a hydrogen diffusion channel [28], allowing hydrogen to be transported to the crack-tip location easily [29]. SFE influences both direct and indirect transformation in metastable steels. The possibility of an indirect transformation phase by $\gamma \rightarrow \varepsilon \rightarrow \alpha'$ increases with further reduction in SFE. It was reported that hydrogen promotes SFE decrease [30–32], resulting in more α′-martensite content. The significant rise in α′-martensite is not entirely due to direct transformation. In other words, both the direct and indirect transformation seems to occur in parallel. It is known from the literature that ε -martensite is only found with plastic deformation in a narrow range of strain between roughly 5% and 40% prior to fracture [33,34]. From the comparison between these results and the uncharged specimen at the strain level of 21% (Fig. 3a and b), It is well understood that hydrogen could change the deformation mechanism. It was observed that hydrogen charging led to an increase in the dislocation density of the current steel, providing direct evidence of hydrogen-enhanced dislocation multiplication during the hydrogen charging. In a model developed by Barnoush et al. [35] based on classical dislocation theory, hydrogen was shown to decrease the activation energy for the nucleation of homogeneous dislocations (HDN). They reported that hydrogen decreased the necessary stress for dislocations nucleation by lowering the shear modulus, dislocation line energy, and SFE.

It has been demonstrated that intergranular fracture occurs due to raising the hydrogen content at grain boundaries. Localized deformation induced by hydrogen at the FCC/BCC and FCC/Cr_2B interfaces led to microcrack propagation. HA also exhibited hydrogen-induced transgranular cracking. Hydrogen could reduce the bonding force of the interfaces, resulting in HE based on the HEDE process [36]. If these events occur within a grain, the decohesion of interface boundaries results in a quasi-cleavage fracture. The production of microcracks at microstructural interfaces after hydrogen charging has previously been described in austenitic stainless

steel [37]. Therefore, the combined impacts of the hydrogen enhanced localized plasticity (HELP) and HEDE processes accelerated crack propagation [38].

The first peak of TDS for both specimens is almost in the same range of 26–31 kJ/mol, which could be interpreted as diffusible or reversible trapping sites. It has been reported in the literature that dislocation, martensite lath, and grain boundary are all types of diffusible or reversible traps with a low-temperature peak [39–41]. It was observed that with the deformation increased, the intensity of the TDS peaks related to diffusible hydrogen (reversible trap) increased. The TDS spectrum showed the increased quality of trap sites after deformation as a results of an increase in the dislocation density. The second peaks of both steels occur at higher temperatures ranging from 334 to 377 °C, which can be considered as non-diffusible hydrogen. The activation energy for the second peak in the undeformed and deformed specimens was 55.6 and 53.9 kJ/mol, respectively. This peak might be related to irreversible traps such as austenite. It should be noted that the calculated activation energy about 55 kJ/mol is near to the binding energy of austenite [42,43]. The corresponding concentration of hydrogen in the deformed specimen was lower than that in the specimen prior to deformation for all heating rates. These results indicated that the undeformed specimen could dissolve more hydrogen than the deformed one. This is due to the fact that the undeformed specimen contains more content of austenite than the deformed specimen. The TRIP effect changed the hydrogen trap condition after deformation. The formation of martensite due to TRIP effect reduced the number of austenite's irreversible hydrogen trap sites while increasing the number of reversible trap sites of martensite. The third peak in the undeformed and deformed specimens had activation energies of 89.7 and 91.4 kJ/mol, respectively. There are a lot of carbides and Cr_2B in the microstructure, as illustrated in Fig. 2. This peak might be due to hydrogen trapped in precipitation. . In any case, traps with binding energies in this range are thought to be irreversible [44], which makes it unlikely that they will cause HE. Precipitation in the microstructure might be regarded as an irreversible trap, however, Precipitations could act as a dislocation pin under deformation and in the presence of hydrogen, providing a local site for hydrogen accumulations [45]. As is seen in Fig. 5, Cr_2B was observed around the crack after hydrogen charging. As consequence of the transformation of austenite into martensite after deformation, TRIP steel has a more complicated hydrogen-trapping behavior than common steels. Deformation diminishes the content of austenite as an irreversible trap via the transformation while increasing reversible trap sites through more dislocations. The intensity of TDS peaks changed as a result of the plastic deformation, which affected the hydrogen trapping sites, according to the combined analysis of microstructure and TDS in this research. In addition, the plastic deformation did not significantly change the temperatures at the peaks, suggesting that the types of trapping sites remained the same.

Based on the literature and the experimental analysis, the effect of hydrogen on the microstructure of the TRIP steel is schematically summarized in Fig. 8. It can be concluded that both plastic deformation and hydrogen charging have the potential to enhance the driving force behind the martensitic transformation. In the uncharged sample, α'-martensite nucleation sites were formed during tensile deformation by slip bands and subsequently, γ was directly transformed into α'. In the H-charged sample, besides the direct transformation, transient ε in the slip bands was formed and finally transformed to α' due to the reduction of SFE by hydrogen. As a result, the deformation-induced transformation occurred both directly and indirectly in the hydrogen environment, leading to

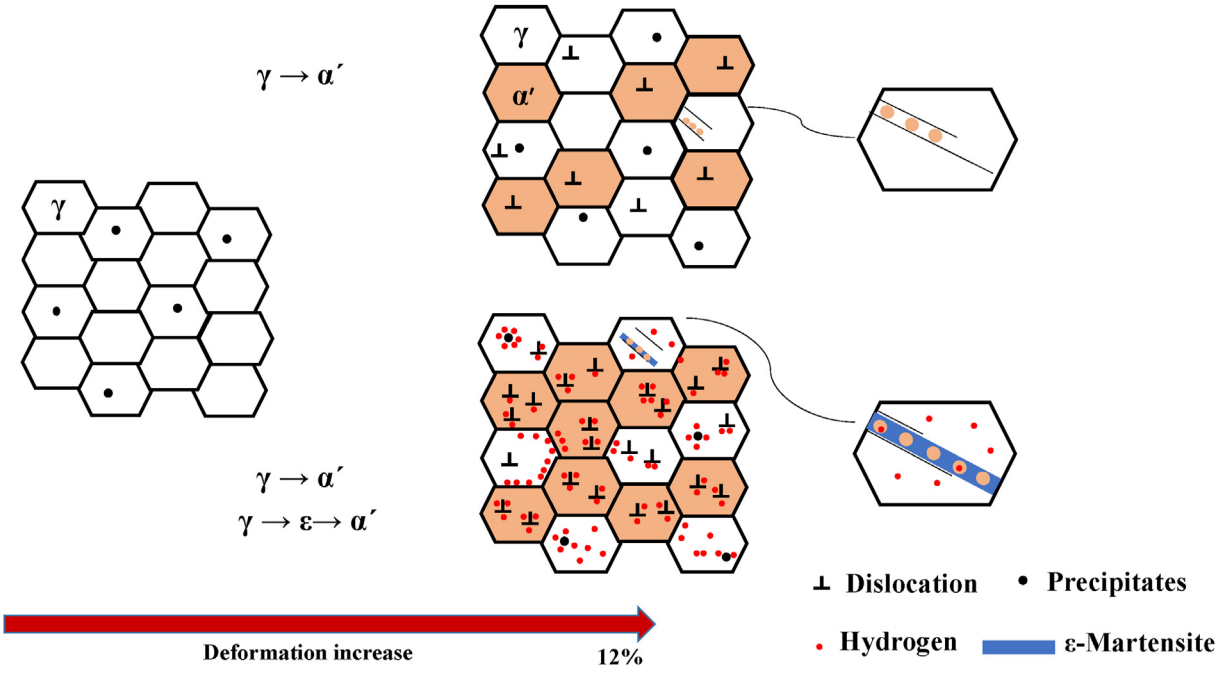

Fig. 8 – A schematic representation of TRIP steel plastic deformation in the presence of hydrogen.

an increase in the proportion of α′-martensite. The transfer of hydrogen to defects by mobile dislocations is a phenomenon that has been demonstrated in several studies [46–48]. Dislocations serve as reversible hydrogen traps, restricting hydrogen diffusion. Hydrogen also improves localized plasticity by facilitating dislocation emission and mobility. Therefore, the higher dislocation density in the H-loaded specimen is one of the reasons that lead to faster failure. The precipitates classified as hydrogen traps had a great impact in the study of HE. The precipitates in TRIP steel serve as irreversible hydrogen traps due to their high binding energy.

5. Conclusion

In the present research, the HE of TRIP steel has been investigated by mechanical properties, microstructure and TDS, The conclusions can be made as follow.

1. The in-situ tensile test showed that the strength and ductility values decreased after hydrogen charging. Moreover, as the current density of hydrogen charging increased, the total strain loss increased to 36%.
2. The EBSD results showed that SFE could be reduced by hydrogen, resulting in both direct and indirect transformation. At the same degree of deformation, the volume proportion of α′- martensite in uncharged and charged samples was 31% and 39%, respectively. In addition, the charged specimen exhibited more dislocations than the uncharged one at the same strain level.
3. Dislocations and austenite lath were found to be reversible and irreversible hydrogen traps by TDS analysis. Precipitates, on the other hand, can be considered irreversible traps. Since more dislocations and martensite were present after plastic deformation, there were more reversible traps in the deformed specimens than in the non-deformed ones.

Declaration of competing interest

The authors declare that they have no known competing financial interests or personal relationships that could have appeared to influence the work reported in this paper.

Acknowledgment

This research is supported by Iran National Science Foundation (INSF) (Grant No. 98005852). The authors would like to thank Ludovica Rovatti for her technical support at Politecnico di Milano.

REFERENCES

[1] Timokhina I, Beladi H, Xiong X-Y, Hodgson PD. On the low temperature strain aging of bainite in the TRIP steel. Metall Mater Trans 2013;44:5177–91.
[2] Zaefferer S, Ohlert J, Bleck W. A study of microstructure, transformation mechanisms and correlation between microstructure and mechanical properties of a low alloyed TRIP steel. Acta Mater 2004;52:2765–78.
[3] Zhou Y, Hojo T, Koyama M, Ajito S, Akiyama E. Synergistic effects of hydrogen and deformation temperature on mechanical properties of TRIP-aided bainitic ferrite steel. Mater Sci Eng, A 2022;842:143070.
[4] Tirumalasetty G, Van Huis M, Kwakernaak C, Sietsma J, Sloof W, Zandbergen H. Deformation-induced austenite grain rotation and transformation in TRIP-assisted steel. Acta Mater 2012;60:1311–21.
[5] Luo Y, Lu H, Min N, Li W, Jin X. Effect of Mo and Nb on mechanical properties and hydrogen embrittlement of hot-rolled medium-Mn steels. Mater Sci Eng, A 2022;844:143108.
[6] Yu X, Zhang X, Wang H, Wang Z, Feng G. High-coverage H2 adsorption on the reconstructed Cu2O (111) surface. J Phys Chem C 2017;121:22081–91.
[7] Feng G, Ganduglia-Pirovano MVn, Huo C-F, Sauer J. Hydrogen spillover to copper clusters on hydroxylated γ-Al2O3. J Phys Chem C 2018;122:18445–55.
[8] Harris ZD, Lawrence SK, Medlin DL, Guetard G, Burns JT, Somerday BP. Elucidating the contribution of mobile hydrogen-deformation interactions to hydrogen-induced intergranular cracking in polycrystalline nickel. Acta Mater 2018;158:180–92.
[9] Schaffner T, Hartmaier A, Kokotin V, Pohl M. Analysis of hydrogen diffusion and trapping in ultra-high strength steel grades. J Alloys Compd 2018;746:557–66.
[10] Behjati A Najafizadeh. Role of chemical driving force in martensitic transformations of high-purity Fe-Cr-Ni alloys. Metall Mater Trans 2011;42:3752–60.
[11] Polatidis E, Hsu W-N, Šmíd M, Panzner T, Chakrabarty S, Pant P, Van Swygenhoven H. Suppressed martensitic transformation under biaxial loading in low stacking fault energy metastable austenitic steels. Scripta Mater 2018;147:27–32.
[12] Ryu JH, Chun YS, Lee CS, Bhadeshia H, Suh DW. Effect of deformation on hydrogen trapping and effusion in TRIP-assisted steel. Acta Mater 2012;60:4085–92.
[13] Fussik R, Egels G, Theisen W, Weber S. Stacking Fault energy in relation to hydrogen environment embrittlement of metastable austenitic stainless CrNi-steels. Metals 2021;11:1170.
[14] Qu W, Gu C, Zheng J, Zhao Y, Hua Z. Effect of plastic deformation at room temperature on hydrogen diffusion of S30408. Int J Hydrogen Energy 2019;44:8751–8.
[15] Luppo M, Ovejero-Garcia J. The influence of microstructure on the trapping and diffusion of hydrogen in a low carbon steel. Corrosion Sci 1991;32:1125–36.
[16] Ronevich J, De Cooman B, Speer J, De Moor E, Matlock D. Hydrogen effects in prestrained transformation induced plasticity steel. Metall Mater Trans 2012;43:2293–301.
[17] Hilditch T, Lee S, Speer J, Matlock D. Response to hydrogen charging in high strength automotive sheet steel products. Society of Automotive Engineers, Inc., Colorado School of Mines; 2003.
[18] Lovicu G, Bottazzi M, D'aiuto F, De Sanctis M, Dimatteo A, Santus C, Valentini R. Hydrogen embrittlement of automotive advanced high-strength steels. Metall Mater Trans 2012;43:4075–87.
[19] Rozenak P, Bergman R. X-ray phase analysis of martensitic transformations in austenitic stainless steels electrochemically charged with hydrogen. Mater Sci Eng, A 2006;437:366–78.
[20] Lacroix G, Pardoen T, Jacques PJ. The fracture toughness of TRIP-assisted multiphase steels. Acta Mater 2008;56:3900–13.
[21] Escobar DP, Verbeken K, Duprez L, Verhaege M. Evaluation of hydrogen trapping in high strength steels by thermal desorption spectroscopy. Mater Sci Eng, A 2012;551:50–8.

[22] Kumar K, Pooleery A, Madhusoodanan K, Singh R, Chakravartty J, Dutta B, Sinha R. Use of miniature tensile specimen for measurement of mechanical properties. Procedia Eng 2014;86:899–909.
[23] Escobar DP, Depover T, Wallaert E, Duprez L, Verhaege M, Verbeken K. Thermal desorption spectroscopy study of the interaction between hydrogen and different microstructural constituents in lab cast Fe–C alloys. Corrosion Sci 2012;65:199–208.
[24] Miresmaeili R, Liu L, Kanayama H. A possible explanation for the contradictory results of hydrogen effects on macroscopic deformation. Int J Pres Ves Pip 2012;99:34–43.
[25] Enos D, Scully J. A critical-strain criterion for hydrogen embrittlement of cold-drawn, ultrafine pearlitic steel. Metall Mater Trans 2002;33:1151–66.
[26] Wang M, Akiyama E, Tsuzaki K. Effect of hydrogen and stress concentration on the notch tensile strength of AISI 4135 steel. Mater Sci Eng, A 2005;398:37–46.
[27] Hirth JP. Effects of hydrogen on the properties of iron and steel. Metall Trans A 1980;11:861–90.
[28] Allam T, Guo X, Lipińska-Chwałek M, Hamada A, Ahmed E, Bleck W. Impact of precipitates on the hydrogen embrittlement behavior of a V-alloyed medium-manganese austenitic stainless steel. J Mater Res Technol 2020;9:13524–38.
[29] Zhang H-y, Zheng L-w, Wang T, Lv W-j, Shi Q-x, Ma J-y, Luo Y, Liang W, Hu J, Misra R. Interrelationship between hydrogen and α'-martensite of SUS 304 austenitic stainless steel revealed by tensile tests. Mater Sci Eng, A 2022;831:142169.
[30] Lu X, Ma Y, Zamanzade M, Deng Y, Wang D, Bleck W, Song W, Barnoush A. Insight into hydrogen effect on a duplex medium-Mn steel revealed by in-situ nanoindentation test. Int J Hydrogen Energy 2019;44:20545–51.
[31] Ke R, Wan X, Zhang Y, Hu C, Wu K. The impact of annealing temperature on the microstructure-Properties relationship of reversion-induced austenitic stainless steels. Mater Sci Eng, A 2022;843:143100.
[32] Lin Y-T, An X, Zhu Z, Nai MLS, Tsai C-W, Yen H-W. Effect of cell wall on hydrogen response in CoCrFeMnNi high-entropy alloy additively manufactured by selective laser melting. J Alloys Compd 2022;925:166735.
[33] Li N, Wang Y, Liu W, An Z, Liu J, Su R, Li J, Liaw P. In situ X-ray microdiffraction study of deformation-induced phase transformation in 304 austenitic stainless steel. Acta Mater 2014;64:12–23.
[34] Spencer K, Véron M, Yu-Zhang K, Embury J. The strain induced martensite transformation in austenitic stainless steels: Part 1–Influence of temperature and strain history. Mater Sci Technol 2009;25:7–17.
[35] Barnoush A, Zamanzade M, Vehoff H. Direct observation of hydrogen-enhanced plasticity in super duplex stainless steel by means of in situ electrochemical methods. Scripta Mater 2010;62:242–5.
[36] Luo H, Zhao B, Pan Z, Fu Y, Li X. Hydrogen induced microstructure evolution and cracking mechanism in a metastable dual-phase high-entropy alloy. Mater Sci Eng, A 2021;819:141490.
[37] Nibur K, Somerday B, Balch D, San Marchi C. The role of localized deformation in hydrogen-assisted crack propagation in 21Cr–6Ni–9Mn stainless steel. Acta Mater 2009;57:3795–809.
[38] Zhao N, Zhao Q, He Y, Liu R, Zheng W, Liu W, Zhang Y. Investigation on hydrogen embrittlement susceptibility in martensitic steels with 1000 MPa yield strength. J Mater Res Technol 2021;15:6883–900.
[39] Liu Y, Chen Y, Yang C, Han X. Study on hydrogen embrittlement and reversibility of hot-stamped aluminized 22MnB5 steel. Mater Sci Eng, A 2022:143411.
[40] Dwivedi SK, Vishwakarma M. Effect of hydrogen in advanced high strength steel materials. Int J Hydrogen Energy 2019;44:28007–30.
[41] Shi R, Chen L, Wang Z, Yang X-S, Qiao L, Pang X. Quantitative investigation on deep hydrogen trapping in tempered martensitic steel. J Alloys Compd 2021;854:157218.
[42] Park Y, Maroef I, Landau A, Olson D. Retained austenite as a hydrogen trap in steel welds, vol. 81. Welding Journal-New York-; 2002. p. 27 [S].
[43] Kim H-J, Lee M-G. Analysis of hydrogen trapping behaviour in plastically deformed quenching and partitioning steel in relation to microstructure evolution by phase transformation. J Alloys Compd 2022;904:164018.
[44] Drexler A, Depover T, Verbeken K, Ecker W. Model-based interpretation of thermal desorption spectra of Fe-C-Ti alloys. J Alloys Compd 2019;789:647–57.
[45] Gong P, Turk A, Nutter J, Yu F, Wynne B, Rivera-Diaz-del-Castillo P, Rainforth WM. Hydrogen embrittlement mechanisms in advanced high strength steel. Acta Mater 2022;223:117488.
[46] Depover T, Verbeken K. The detrimental effect of hydrogen at dislocations on the hydrogen embrittlement susceptibility of Fe-CX alloys: an experimental proof of the HELP mechanism. Int J Hydrogen Energy 2018;43:3050–61.
[47] Robertson I, Birnbaum H, Sofronis P. Hydrogen effects on plasticity. Dislocations in solids 2009;15:249–93.
[48] Chen W, Zhao W, Gao P, Li F, Kuang S, Zou Y, Zhao Z. Interaction between dislocations, precipitates and hydrogen atoms in a 2000 MPa grade hot-stamped steel. J Mater Res Technol 2022;18:4353–66.